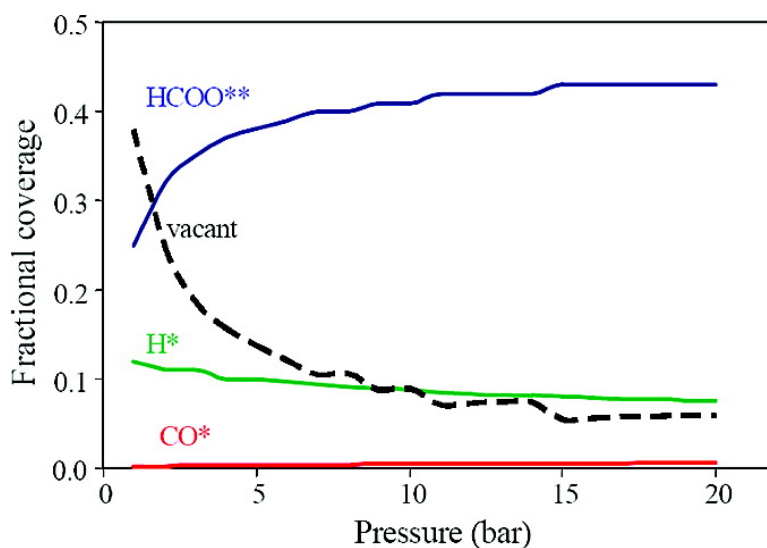Article

On the Mechanism of Low-Temperature Water Gas Shift Reaction on Copper

Amit A. Gokhale, James A. Dumesic, and Manos Mavrikakis

More About This Article

Additional resources and features associated with this article are available within the HTML version:

- Supporting Information
- Links to the 7 articles that cite this article, as of the time of this article download
- Access to high resolution figures
- Links to articles and content related to this article
- Copyright permission to reproduce figures and/or text from this article

View the Full Text HTML

On the Mechanism of Low-Temperature Water Gas Shift Reaction on Copper

Amit A. Gokhale, James A. Dumesic, and Manos Mavrikakis*

Department of Chemical and Biological Engineering, University of Wisconsin-Madison, Madison, Wisconsin 53706

Received September 9, 2007; E-mail: manos@engr.wisc.edu

Abstract: Periodic, self-consistent density functional theory (DFT-GGA) calculations are used to investigate the water gas shift reaction (WGSR) mechanism on Cu(111). The thermochemistry and activation energy barriers for all the elementary steps of the commonly accepted redox mechanism, involving complete water activation to atomic oxygen, are presented. Through our calculations, we identify carboxyl, a new reactive intermediate, which plays a central role in WGSR on Cu(111). The thermochemistry and activation energy barriers of the elementary steps of a new reaction path, involving carboxyl, are studied. A detailed DFT-based microkinetic model of experimental reaction rates, accounting for both the previous and the new WGSR mechanism show that, under relevant experimental conditions, (1) the carboxyl-mediated route is the dominant path, and (2) the initial hydrogen abstraction from water is the rate-limiting step. Formate is a stable "spectator" species, formed predominantly through CO_2 hydrogenation. In addition, the microkinetic model allows for predictions of (i) surface coverage of intermediates, (ii) WGSR apparent activation energy, and (iii) reaction orders with respect to CO, H_2O, CO_2, and H_2.

Introduction

The water gas shift reaction (WGSR), namely, CO + H_2O → CO_2 + H_2, is an industrially important reaction for H_2 production. In addition, WGSR or its reverse is directly or indirectly relevant to several current industrial catalytic technologies such as methanol (MeOH) synthesis,[1-3] MeOH steam reforming,[4-6] ammonia synthesis,[7] coal gasification, and catalytic combustion. Large-scale production of H_2, as envisioned for the hydrogen economy, for instance in connection with hydrogen fuel cells,[4-6,8-14] has sparked renewed interest in finding improved WGSR catalysts. WGSR is mildly exothermic, suggesting that it is thermodynamically favored at lower temperatures. However, because of kinetic limitations, faster reaction rates would be achievable at higher temperatures. In practice, WGSR is typically carried out in two steps: the high-temperature stage employing iron oxide-based catalysts, and the

low-temperature stage employing copper-based catalysts.[15-18] Given the goal of the present work, we will focus our subsequent discussion on the low-temperature WGSR.

Because of the broad range of applications and the importance of this reaction, a number of experimental[10,16,18-34] and theoretical[13,14,35,36] studies have been conducted to elucidate the reaction

(1) Askgaard, T. S.; Nørskov, J. K.; Ovesen, C. V.; Stoltze, P. *J. Catal.* **1995**, *156*, 229.
(2) Rozovskii, A. Y.; Lin, G. I. *Top. Catal.* **2003**, *22*, 127.
(3) Kurz, E. A.; Hudson, J. B. *Surf. Sci.* **1988**, *195*, 15.
(4) Velu, S.; Suzuki, K.; Kapoor, M. P.; Ohashi, F.; Osaki, T. *Appl. Catal., A* **2001**, *213*, 47.
(5) Choi, Y.; Stenger, H. G. *Appl. Catal., B* **2002**, *38*, 259.
(6) Geissler, K.; Newson, E.; Vogel, F.; Truong, T.-B.; Hottinger, P.; Wokaun, A. *Phys. Chem. Chem. Phys.* **2001**, *3*, 289.
(7) Carstensen, J. H.; Hansen, J. B.; Pedersen, P. S. *Ammonia Plant Saf.* **1991**, *31*, 113.
(8) Ruettinger, W.; Ilinich, O.; Farrauto, R. J. *J. Power Sources* **2003**, *118*, 61.
(9) Godat, J.; Marechal, F. *J. Power Sources* **2003**, *118*, 411.
(10) Koryabkina, N. A.; Phatak, A. A.; Ruettinger, W. F.; Farruto, R. J.; Rebeiro, F. H. *J. Catal.* **2003**, *217*, 233.
(11) Zalc, J. M.; Sokolovskii, V.; Loeffler, D. G. *J. Catal.* **2002**, *206*, 169.
(12) Cortright, R. D.; Davda, R. R.; Dumesic, J. A. *Nature* **2002**, *418*, 964.
(13) Liu, P.; Rodriguez, J. A. *J. Chem. Phys.* **2007**, *126*, 164705.
(14) Rodriguez, J. A.; Liu, P.; Hrbek, J.; Evans, J.; Perez, M. *Angew. Chem., Int. Ed.* **2007**, *46*, 1329.

(15) Chorkendorff, I.; Niemantsverdriet, H. *Concepts of Modern Catalysis and Kinetics;* Wiley-VCH: Weinheim, Germany, 2003.
(16) Ovesen, C. V.; Stoltze, P.; Nørskov, J. K.; Campbell, C. T. *J. Catal.* **1992**, *134*, 445.
(17) Ovesen, C. V.; Clausen, B. S.; Hammershøi, B. S.; Steffensen, G.; Askgaard, T.; Chorkendorff, I.; Nørskov, J. K.; Rasmussen, P. B.; Stoltze, P.; Taylor, P. *J. Catal.* **1996**, *158*, 170.
(18) Campbell, C. T.; Ernst, K. H. *Surface science of catalysis: In situ probes and reaction kinetics;* Dwyer, D. J., Hoffmann, F. M., Eds.; ACS Symposium Series 482; American Chemical Society: Washington, DC, 1992; p 130.
(19) Grenoble, D. C.; Estadt, M. M.; Ollis, D. F. *J. Catal.* **1981**, *67*, 90.
(20) Ovesen, C. V.; Clausen, B. S.; Schiotz, J.; Stolze, P.; Topsøe, H.; Nørskov, J. K. *J. Catal.* **1997**, *168*, 133.
(21) Campbell, C. T.; Daube, K. A. *J. Catal.* **1987**, *104*, 109.
(22) Campbell, C. T.; Koel, B. E.; Daube, K. A. *J. Vac. Sci. Technol., A* **1987**, *5*, 810.
(23) Ernst, K.-H.; Campbell, C. T.; Moretti, G. *J. Catal.* **1992**, *134*, 66.
(24) Hinrichsen, O.; Genger, T.; Muhler, M. *Stud. Surf. Sci. Catal.* **2000**, *130*, 3825.
(25) Xue, E.; O'Keeffe, M.; Ross, J. R. H. *Catal. Today* **1996**, *30*, 107.
(26) Capek, P.; Klusacek, K. *Catal. Today* **1994**, *20*, 367.
(27) Nakamura, J.; Cambell, J. M.; Campbell, C. T. *J. Chem. Soc., Faraday Trans.* **1990**, *86*, 2725.
(28) Chen, C.-S.; Cheng, W.-H.; Lin, S.-S. *Appl. Catal., A* **2003**, *238*, 55.
(29) Chen, C.-S.; Cheng, W.-H. *Catal. Lett.* **2002**, *83*, 121.
(30) Tserpe, E.; Waugh, K. C. *Stud. Surf. Sci. Catal.* **1997**, *109*, 401.
(31) Shido, T.; Iwasawa, Y. *J. Catal.* **1993**, *140*, 575.
(32) Campbell, C. T. Promoters and Poisons in the Water-Gas Shift Reaction. In *The Chemical Physics of Solid Surfaces and Heterogeneous Catalysis;* King, D. A., Woodruff, D. P., Eds.; Elsevier: Amsterdam, 1993; Vol. 6; p 287.
(33) Yoshihara, J.; Parker, S.; Schafer, A.; Campbell, C. T. *Catal. Lett.* **1995**, *31*, 313.
(34) Yoshihara, J.; Campbell, C. T. *J. Catal.* **1996**, *161*, 776.
(35) Wang, G.; Jiang, L.; Cai, Z.; Pan, Y.; Zhao, X.; Huang, W.; Xie, K.; Li, Y.; Sun, Y.; Zhong, B. *J. Phys. Chem. B* **2003**, *107*, 557.

mechanism and to investigate the role of promoters and poisons.[22,25,31] Despite these numerous studies, the exact reaction mechanism remains unsettled. Redox mechanisms involving CO oxidation by adsorbed atomic O, obtained either by the direct two-step water dissociation[18,27] or by the disproportionation of OH,[10,16,17] a species generated by single H abstraction from water, have been proposed. Furthermore, formate species[21,22,33,37,38] (HCOO**), presumably formed by the reaction of adsorbed CO and OH, have been discussed extensively as a key reactive intermediate. Formate has been detected experimentally within the framework of IRAS, HREELS, STM, and EXAFS studies.[39-43]

In this study, we perform a periodic self-consistent DFT investigation of the WGSR on Cu(111), the dominant facet of active WGSR industrial catalytic nanoparticles. We determine the thermochemistry and detailed energetic aspects of the kinetics for the elementary steps involved in the redox mechanism. Furthermore, we propose a new mechanism for the WGSR involving a highly reactive surface intermediate, carboxyl (COOH), and we determine the thermochemistry and activation energy barriers of the elementary steps in this new mechanism. Given prior suggestions that metallocarboxylic acids play an active role in homogeneous WGSR,[44-46] our new COOH-mediated mechanism for the heterogeneous WGSR may provide a direct link between homogeneous and heterogeneous catalysis for a key industrial catalytic process.

The DFT-derived parameters, including binding energies, activation energy barriers, entropies, and pre-exponential factors, are all used subsequently for developing a detailed microkinetic model[47-49] that accounts for both the redox and COOH-mediated WGSR mechanisms. Published experimentally measured WGSR rates[10,38] are then compared to reaction rates predicted by our microkinetic model, and we show that, under typical WGSR conditions, the COOH-mediated mechanism is the dominant reaction route for Cu-based heterogeneous WGSR catalysis.

Methods

DACAPO, the total energy calculation code,[50,51] is used for all DFT calculations in this study. A three-layer Cu slab with a 2×2 surface unit cell, periodically repeated in a supercell geometry with five equivalent layers of vacuum between any two successive metal slabs, is used to model Cu(111). Adsorption is allowed on only one of the two surfaces exposed, and the electrostatic potential is adjusted accordingly.[52,53] Our systematic investigations determined that surface

(36) Jakdetchai, O.; Nakajima, T. *J. Mol. Struct.: THEOCHEM* **2002**, *619*, 51.
(37) Herwijnen, T. V.; Jong, W. A. D. *J. Catal.* **1980**, *63*, 94.
(38) Herwijnen, T. V.; Jong, W. A. D. *J. Catal.* **1980**, *63*, 83.
(39) Fujitani, T.; Choi, Y.; Sano, M.; Kushida, Y.; Nakamura, J. *J. Phys. Chem. B* **2000**, *104*, 1235.
(40) Hayden, B. E.; Prince, K.; Woodruff, D. P.; Bradshaw, A. M. *Surf. Sci.* **1983**, *133*, 589.
(41) Sexton, B. A.; Huges, A. E.; Avery, N. R. *Surf. Sci.* **1985**, *155*, 366.
(42) Dubois, L. H.; Ellis, T. H.; Zegarski, B. R.; Kevan, S. D. *Surf. Sci.* **1986**, *172*, 385.
(43) Crapper, M. D.; Riley, C. E.; Woodruff, D. P.; Puschmann, A.; Haase, J. *Surf. Sci.* **1986**, *171*, 1.
(44) Laine, R. M.; Crawford, E. J. *J. Mol. Catal.* **1988**, *44*, 357.
(45) Rice, S. F.; Steeper, R. R.; Aiken, J. D. *J. Phys. Chem. A* **1998**, *102*, 2673.
(46) Darensbourg, D. J.; Froelich, J. A. *J. Am. Chem. Soc.* **1977**, *99*, 4727.
(47) Dumesic, J. A.; Rudd, D. F.; Aparicio, L. M.; Rekoske, J. E.; Trevino, A. A. *The Microkinetics of Heterogeneous Catalysis;* American Chemical Society: Washington, DC, 1993.
(48) Cortright, R. D.; Dumesic, J. A. *Adv. Catal.* **2001**, *46*, 161.
(49) Gokhale, A. A.; Kandoi, S.; Greeley, J. P.; Dumesic, J. A.; Mavrikakis, M. *Chem. Eng. Sci.* **2004**, *59*, 4679.
(50) Hammer, B.; Hansen, L. B.; Nørskov, J. K. *Phys. Rev. B* **1999**, *59*, 7413.
(51) Greeley, J.; Nørskov, J. K.; Mavrikakis, M. *Annu. Rev. Phys. Chem.* **2002**, *53*, 319.
(52) Neugebauer, J.; Scheffler, M. *Phys. Rev. B* **1992**, *46*, 16067.
(53) Bengtsson, L. *Phys. Rev. B* **1999**, *59*, 12301.

Table 1. Redox Mechanism vs Carboxyl Mechanism for WGSR on Cu(111)[a]

redox mechanism	carboxyl mechanism
CO + * → CO*	CO + * → CO*
H₂O + * → H₂O*	H₂O + * → H₂O*
H₂O* + * → H* + OH*	H₂O* + * → H* + OH*
OH + * → O* + H**	*CO* + OH* → COOH* + **
OH + OH* → H₂O* + O*	*COOH* + * → CO₂* + H**
CO + O* → CO₂* + **	*COOH* + OH* → CO₂* + H₂O**
CO₂* → CO₂ + *	CO₂* → CO₂ + *
H* + H* → H₂ + 2*	H* + H* → H₂ + 2*

$CO + * \rightarrow CO^*$ $CO + * \rightarrow CO^*$
$H_2O + * \rightarrow H_2O^*$ $H_2O + * \rightarrow H_2O^*$
$H_2O^* + * \rightarrow H^* + OH^*$ $H_2O^* + * \rightarrow H^* + OH^*$
$OH^* + * \rightarrow O^* + H^*$ *$CO^* + OH^* \rightarrow COOH^* + *$*
$OH^* + OH^* \rightarrow H_2O^* + O^*$ *$COOH^* + * \rightarrow CO_2^* + H^*$*
$CO^* + O^* \rightarrow CO_2^* + *$ *$COOH^* + OH^* \rightarrow CO_2^* + H_2O^*$*
$CO_2^* \rightarrow CO_2 + *$ $CO_2^* \rightarrow CO_2 + *$
$H^* + H^* \rightarrow H_2 + 2*$ $H^* + H^* \rightarrow H_2 + 2*$

[a] Steps in italics highlight differences between the two mechanisms. * Indicates a vacant site. X* denotes an adsorbed X species.

relaxation has a very small effect on the energetics of adsorption, and to limit the size of the calculations, all the copper atoms are kept fixed at their bulk-truncated positions. Ionic cores are described by ultrasoft pseudopotentials,[54] and the Kohn–Sham one-electron valence states[55] are expanded in a basis of plane waves with kinetic energy below 25 Ry. The surface Brillouin zone is sampled at 18 special **k** points,[56] and convergence of the total energy with respect to the number of metal layers included is confirmed. The exchange-correlation energy and potential are described by the generalized gradient approximation (GGA-PW91).[57,58] Zero-point energy corrections are not included in the reported results unless otherwise indicated. The calculated PW91 lattice constant for bulk Cu is found to be 3.66 Å, in good agreement with the experimental value (3.62 Å).[59]

The climbing-image nudged elastic band method has been used to determine the minimum energy paths for all the elementary steps.[60-62] The transition state of the optimized reaction coordinate is approximated by the image of highest energy. A vibrational frequency analysis[63] is subsequently used to verify the uniqueness of a negative mode, confirming the true nature of the saddle point.

Athena visual workbench, a nonlinear differential equation solver capable of nonlinear parameter estimation developed by Stewart and co-workers,[64] is used for microkinetic modeling of two sets of experimental WGSR data. The binding energies and entropies of the adsorbed species, and the pre-exponential factors and activation energies of the elementary steps as derived from DFT, are all used as parameters in the microkinetic model.

Results

Reaction Mechanism. The redox mechanism outlined in Table 1 is currently the most accepted mechanism for WGSR. This mechanism involves the oxidation of CO by atomic O obtained from H_2O either by two successive H abstraction steps (labeled as dissociation) or by one H abstraction followed by disproportionation of two OH species (labeled as disproportionation). Table 1 also introduces our proposal for an alternative WGSR mechanism, involving the oxidation of CO by OH, to form *carboxyl* (COOH) species. Carboxyl so formed may then yield CO_2. We will refer to the mechanism proceeding via

(54) Vanderbilt, D. *Phys. Rev. B* **1990**, *41*, 7892.
(55) Kohn, W.; Sham, L. J. *Phys. Rev.* **1965**, *140*, A1133.
(56) Chadi, D. J.; Cohen, M. L. *Phys. Rev. B* **1973**, *8*, 5747.
(57) Perdew, J. P.; Chevary, J. A.; Vosko, S. H.; Jackson, K. A.; Pederson, M. R.; Singh, D. J.; Fiolhais, C. *Phys. Rev. B* **1992**, *46*, 6671.
(58) White, J. A.; Bird, D. M.; Payne, M. C.; Stich, I. *Phys. Rev. Lett.* **1994**, *73*, 1404.
(59) *CRC Handbook of Chemistry and Physics,* 76th ed.; CRC Press: New York, 1996.
(60) Henkelman, G.; Uberuaga, B. P.; Jónsson, H. *J. Chem. Phys* **2000**, *113*, 9901.
(61) Jónsson, H. J.; Mills, G.; Jacobsen, K. W. *In Classical and Quantum Dynamics in Condensed Phase Simulations;* World Scientific: Singapore, 1998.
(62) Henkelman, G.; Jónsson, H. *J. Chem. Phys.* **2000**, *113*, 9978.
(63) Greeley, J.; Mavrikakis, M. *Surf. Sci.* **2003**, *540*, 215.
(64) Stewart, W. E.; Caracotsios, M.; Sorensen, J. P. *AIChE J.* **1992**, *38*, 641.

Table 2. Binding Energies and Geometric Parameters for WGSR Intermediates on Cu(111)[a]

Atomic Adsorbates

Species	Preferred Site	Binding Energy (eV)		Vibrational modes (cm^{-1})	S J/mol K	Cu – A (Å)	A$_z$ (Å)
		without ZPEC	with ZPEC				
H	Fcc / Hcp	-2.55	-2.38 (-2.47)	1015, 873, 878	21.54	1.75	0.90
O	Fcc	-4.41	-4.34	All modes below 500 cm^{-1}	39.60	1.97	1.19

Diatomic adsorbates

Species	Preferred Site	Binding Energy (eV)		Vibrational modes (cm^{-1})	S J/mol K	Bonded to Cu through (atom A)	Cu – A (Å)	A$_z$ (Å)	Bond Length (Å)
		without ZPEC	with ZPEC						
CO	Fcc / Hcp	-0.96	-0.94	1922	85.56	Carbon	2.08	1.41	1.19
OH	Fcc / Hcp	-2.85	-2.77 (-2.80)	3702	72.44	Oxygen	2.06	1.43	0.98

Polyatomic Adsorbates

Species	Preferred Site	Vibrational modes (cm^{-1})	Binding Energy (eV)		S J/mol K	Bonded to Cu through (atom A)	Cu–A in Å	A$_z$ in Å	Bond Details	
			without ZPEC	with ZPEC					Bond	Bond Length (Å)
cis-carboxyl	Top	3637, 1749, 893,1106, 524, 595	-1.68	-1.64	129.49	Carbon	1.96	1.94	C – O	1.40
									C=O	1.22
									O – H	0.99
Trans-carboxyl	Off - top	3574, 1504, 1233, 1135, 689, 671	-1.88	-1.84	114.99	Carbon	1.99	1.87	C – O	1.34
									C=O	1.26
									O – H	0.99
Unidentate formate	Hcp	2938, 1756, 1321, 980, 1110, 697	-2.32	-2.18	124.54	Oxygen	2.11	1.51	C – O	1.35
									C=O	1.22
									C – H	1.11
Bidentate formate	Top – Top through O	2890, 1572, 1298, 1352, 990, 746	-2.77	-2.62 (-2.72)	115.01	2 Oxygen atoms	2.04	2.03	C – O	1.27
									C – H	1.11
CO$_2$	Top - linear	2333, 1285, 670, 663	-0.09	-0.09	116.82	Carbon	3.67	3.67	C – O	1.18
H$_2$O	Top - flat	3919 , 3715, 1548	-0.18	-0.13	102.70	Oxygen	2.81	2.79	O – H	0.99

[a] Binding energies with and without zero-point energy correction (ZPEC) are given. The binding energies with ZPEC are used in the microkinetic model. Shaded entries represent the values that needs to be changed to fit the microkinetic model to the experimental data, whereas entries in parentheses indicate the value used in that model. The DFT-calculated vibrational modes and the entropy, S, calculated from these frequencies are also provided. Although only the vibrational modes above 500 cm^{-1} are shown here, entropies have been calculated using all calculated modes. Cu−A denotes the metal−atom bond length, and A$_z$ denotes the vertical distance of the adsorbate from the slab's surface. Bond angles for polyatomic adsorbates are shown in Figure 1.

COOH as the "carboxyl mechanism". Previous studies[22] have suggested that CO and OH can react to form a bidentate formate (HCOO) species which then decomposes to CO$_2$ and H. We note that COOH and HCOO are isomers of each other. However, as we will show later on, although it is possible to form COOH from CO and OH in a single elementary reaction step, that is not possible with HCOO formation. That is because OH binds to the surface through its O atom, CO through its C atom, whereas formate binds through its two O atoms, not its C atom.

Our studies suggest that the easiest way to form HCOO, a spectator species for the WGSR, is by reacting CO$_2$ with atomic H.

Structure and Energetics of Absorbed Intermediates. The adsorption characteristics of all the surface intermediates involved in the reaction mechanisms shown in Table 1 are studied. Our findings regarding the binding energy (BE), bonding configuration, bond lengths, and the vibrational fre-
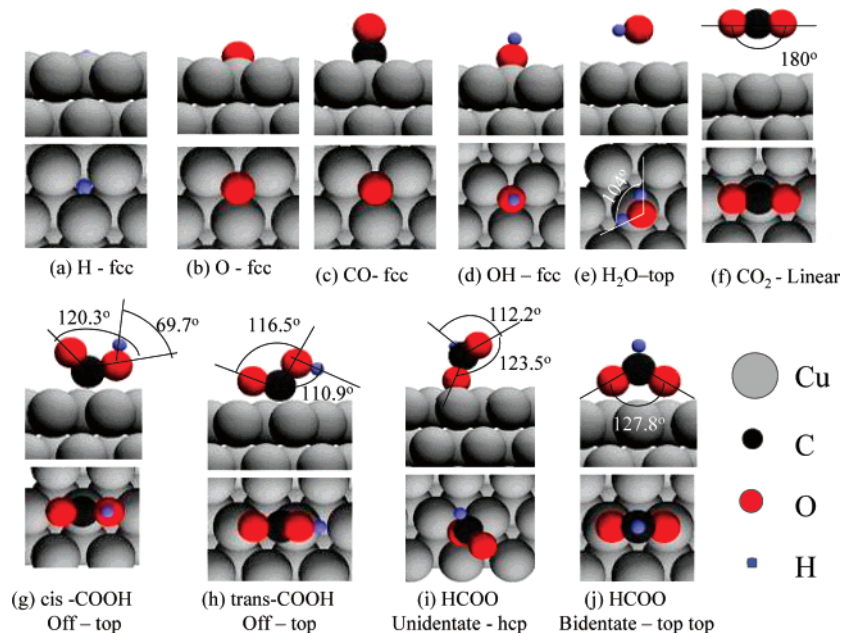
Figure 1. Most stable configurations of WGSR intermediates on Cu(111). Top and bottom panels for each pair of images provide a cross section and an on-top view of the slabs, respectively. Internal bond angles for polyatomic adsorbates are also shown. Table 2 provides further geometric details for these structures.

quencies for the energetically preferred states are summarized in Table 2; Figure 1 shows schematics of those states.

Our results show that *atomic hydrogen* binds equally strong at the fcc (Figure 1a) and the hcp sites. *Atomic oxygen* shows a clear preference for the fcc site (Figure 1b). Referred to gas-phase atoms, the binding energies of H and O on Cu(111) are -2.55 and -4.41 eV, respectively. CO adsorption is isoenergetic for the fcc (Figure 1c) and hcp sites with a BE of -0.96 eV. CO adsorbs at these sites perpendicular to the surface with the C-end toward the surface. Similarly, OH binds isoenergetically to the fcc (Figure 1c) and hcp sites (BE = -2.85 eV), with its axis perpendicular to the surface. *Water* and *carbon dioxide* adsorb weakly with BE values of -0.18 and -0.09 eV, respectively (Figure 1e,f).

Carboxyl (COOH) exhibits two stable structures on Cu(111) (Figure 1g,h): (i) one with the O—H bond pointing away from the surface (*cis*-COOH) and a BE of -1.68 eV, and (ii) one with the O—H bond pointing toward the surface (*trans*-COOH) with a BE of -1.88 eV. Since the *trans*-COOH species is more stable, hereon we use the term carboxyl to refer to this species, unless otherwise stated. Adsorbed *formate* (HCOO) also shows two stable structures, namely unidentate (Figure 1i) and bidentate (Figure 1j). The unidentate HCOO has a BE of -2.32 eV, whereas the bidentate HCOO is significantly more stable with a BE of -2.77 eV. Adsorbed COOH and HCOO states are isomers of each other, with the bidentate HCOO being the thermodynamically more stable species on Cu(111) by ca. 0.6 eV.

Activation Energy Barriers

In this section, we will describe the characteristics of the minimum energy path we identified for each one of the elementary steps considered in this study (Figures 2−6). In addition, Table 3 summarizes bond lengths, vibrational frequencies, and energetics of the transition states, as well as calculated

values for frequency factors. Finally, Figure 7 compares the various pathways for WGSR on Cu(111) based on the energetics of these steps.
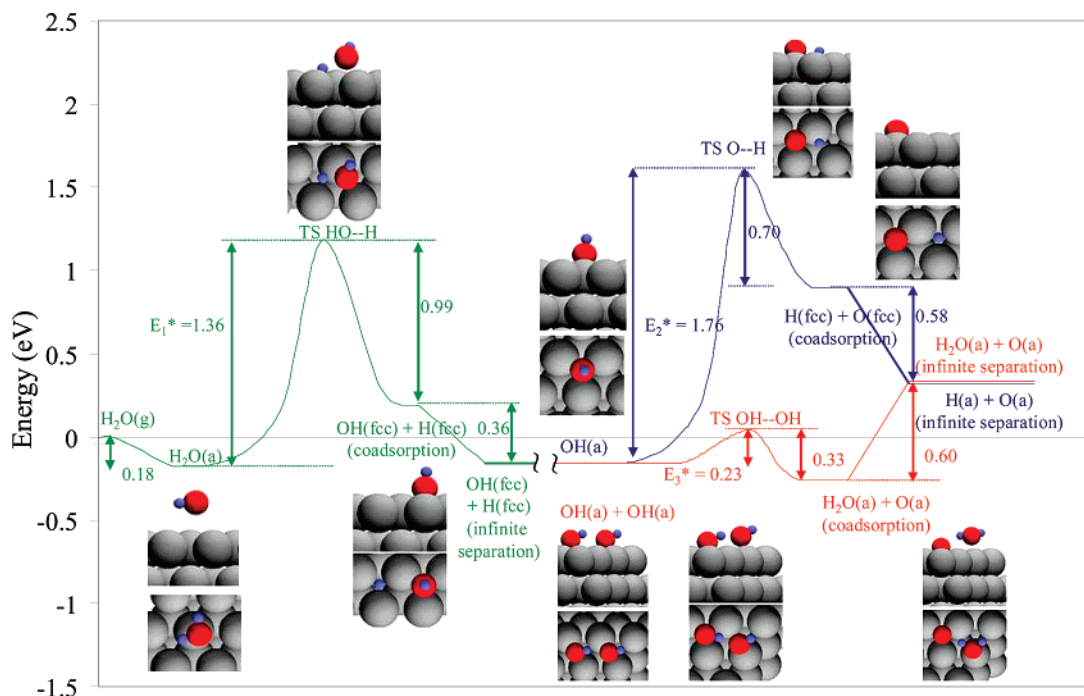
1. Water Activation on Cu(111).

1.1. First H Abstraction from H$_2$O (H$_2$O* + * → H* + OH*). This step is practically thermoneutral ($\Delta E = 0.01$ eV) but with an activation energy of 1.36 eV (Table 3). Figure 2 (green line) shows the respective reaction coordinate. The most favorable pathway involves H abstraction from H$_2$O over the bridge site, giving H and OH coadsorbed at fcc sites. At the transition state, both H and OH are at bridge sites, separated by a distance of 2.23 Å.

1.2. OH Dissociation (OH* + * → O* + H*). The OH dissociation step is endothermic by 0.48 eV. Figure 2 (blue line) shows the minimum energy path for this elementary step. The initial state involves OH at the fcc site, with the O—H axis almost perpendicular to the surface. In the final, coadsorbed state, O and H occupy fcc sites. Coadsorbed O and H repel each other by 0.58 eV. The activation energy barrier for OH dissociation is 1.76 eV. The distance between O and H at the transition state is 1.61 Å (Table 3), and the O and H atoms are above the fcc and bridge sites, respectively (Figure 2).

1.3. OH + OH Disproportionation (OH* + OH* → H$_2$O* + O*). An alternative path for producing atomic oxygen on Cu(111) is offered by OH disproportionation. Coadsorbed OH species prefer the bridge-tilted orientation (Figure 2). When coadsorbed, the products of this step, H$_2$O and O, attract each other by a remarkable 0.60 eV. Our minimum energy path calculations suggest that this is a very facile step, with an activation energy barrier of only 0.23 eV.

2. CO Oxidation on Cu(111).

2.1. CO Oxidation by Atomic O (CO* + O* → CO$_2$* + *). CO oxidation by atomic O is highly exothermic ($\Delta E = -0.87$ eV). When by itself, CO prefers to adsorb at the fcc site, but when coadsorbed with O, CO prefers to move to a top

Figure 2. Water activation steps on Cu(111). First H abstraction from water is shown in green. The competitive steps of OH dissociation and OH disproportionation are shown in blue and red, respectively; to facilitate comparison, the initial states for these two steps are taken to have the same energy. Top and bottom panels of the insets provide a cross section and a top view, respectively, of the initial state, transition state, and final state for each step. Zero of the energy scale corresponds to the energy of gas-phase H_2O at infinite separation from the slab. ZPEs are not included. E_1^*, E_2^*, and E_3^* denote the activation energy for first H abstraction from H_2O, OH dissociation, and OH disproportionation reaction, respectively.
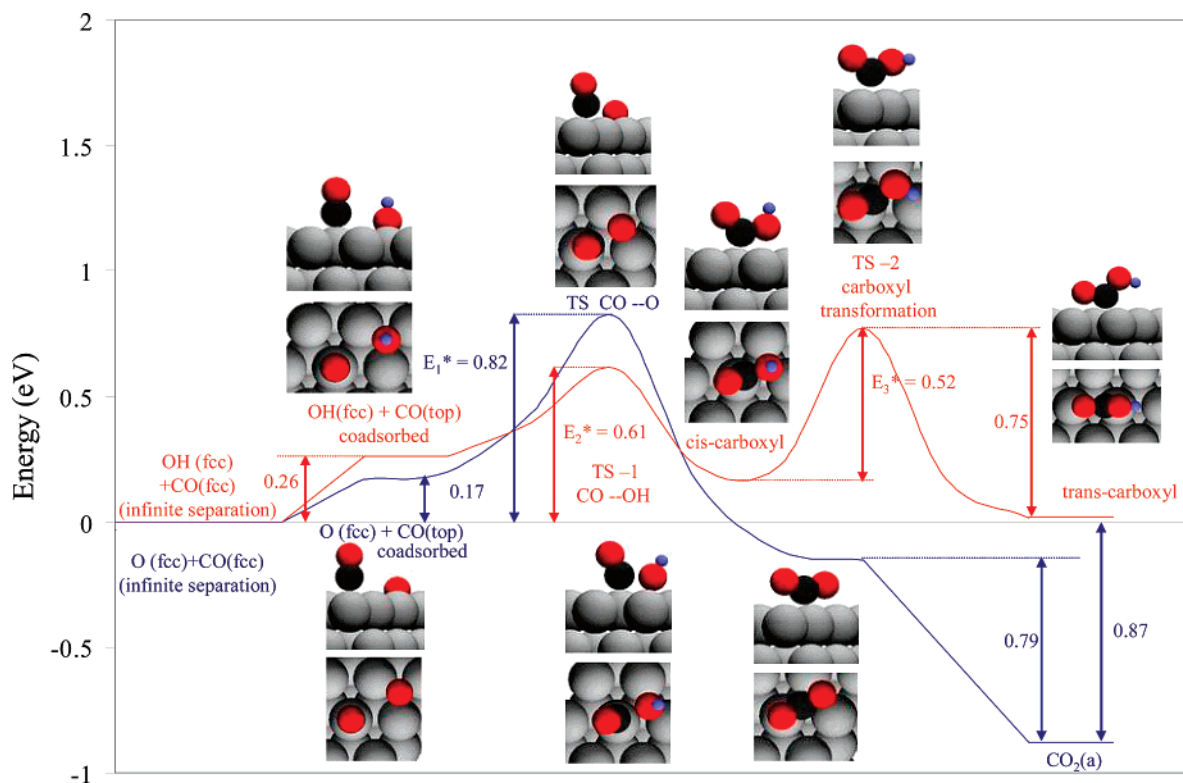
Figure 3. CO oxidation on Cu(111). The competitive minimum energy paths for CO oxidation by O and OH are shown with blue and red lines, respectively; for direct comparison, their initial states are taken to have the same energy. Top and bottom panels of each inset provide a cross section and a top view, respectively, of the initial coadsorbed states, final states, and transition states for each step. Zero of the energy scale corresponds to the energy of CO and O or CO and OH adsorbed at infinite separation on the slab. ZPEs are not included. E_1^* denotes the activation energy for CO oxidation by O, while E_2^* and E_3^* denote the activation energy for *cis*-carboxyl and subsequent *trans*-carboxyl formation steps, respectively.

site. In variance with that CO behavior, upon coadsorption with CO, atomic O retains its preference for the fcc site (Figure 3).

The transition state is characterized by O at a bridge site and CO in a tilted configuration slightly off a top site (Figure 3).
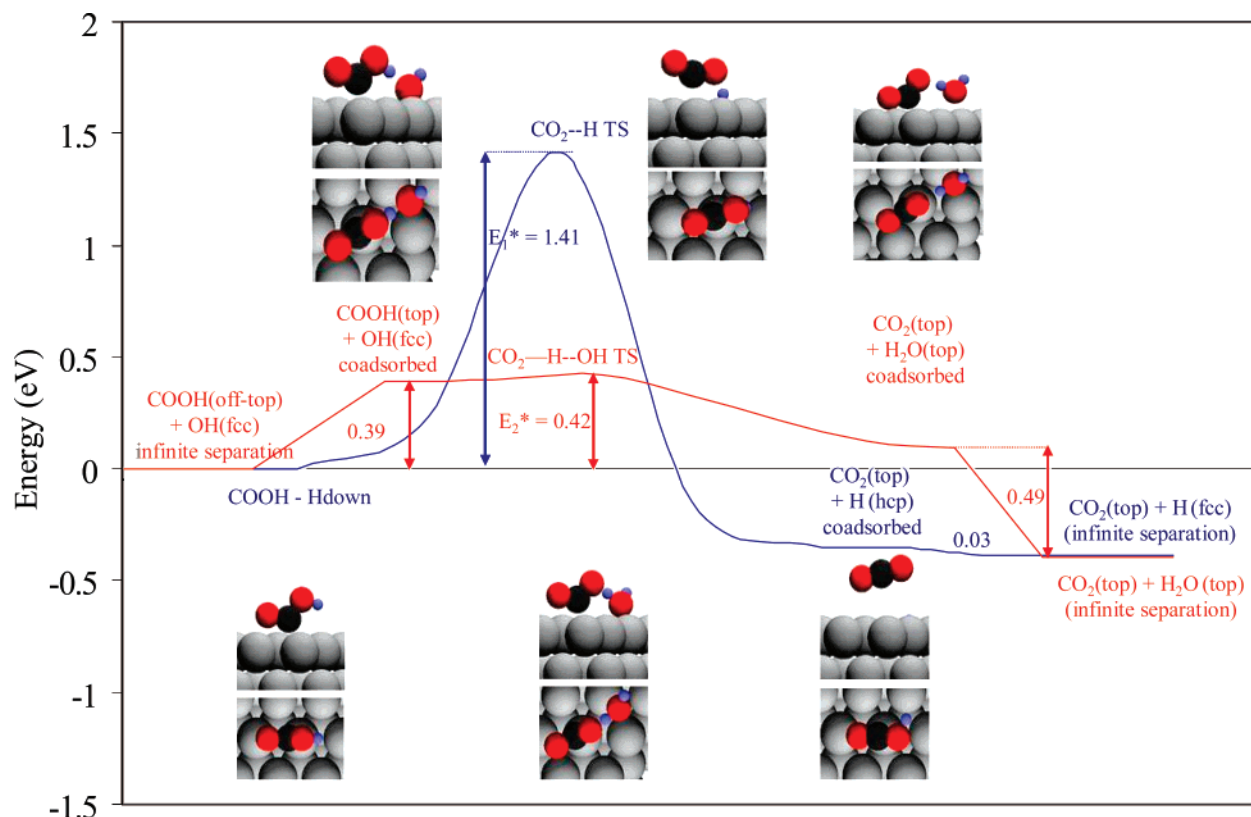
Figure 4. Carboxyl decomposition. Alternative steps for carboxyl decomposition:direct dissociation and disproportionation by OH are shown with blue and red lines, respectively. For direct comparison of the two alternatives, the initial states of both steps are taken as having the same energy. Top and bottom panels of the each inset provide a cross section and a top view, respectively, of the initial coadsorbed states, transition states, and final states for each step. Zero of the energy scale corresponds to the energy of adsorbed carboxyl or of carboxyl plus OH adsorbed at infinite separation on the slab, for the two colored lines, respectively. ZPEs are not included. E_1^* and E_2^* denote the activation energies for carboxyl dissociation and carboxyl disproportionation by OH, respectively.
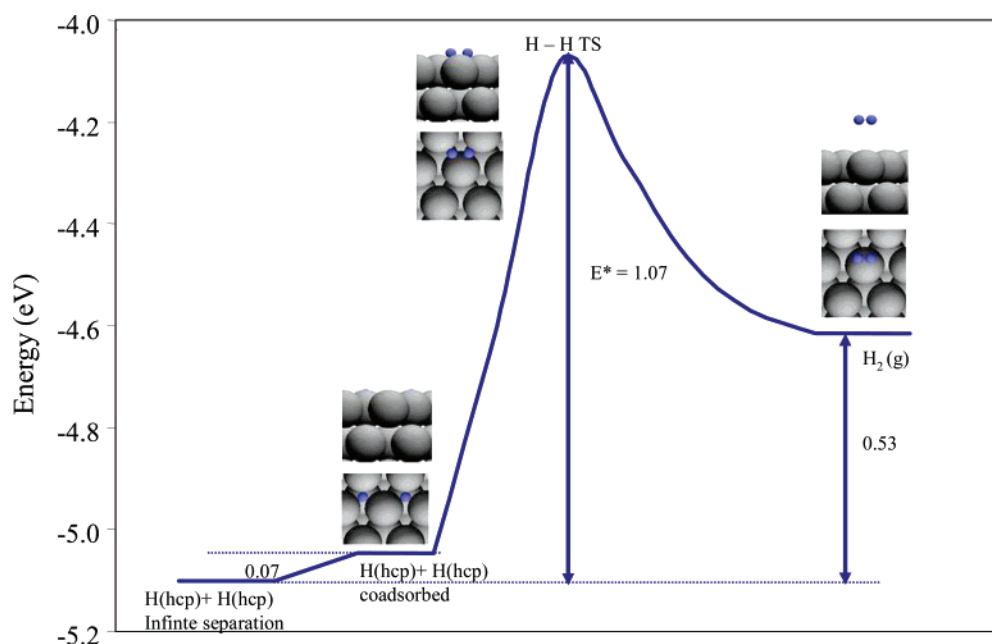
Figure 5. H_2 recombinative desorption. Reaction coordinate for H_2 recombination. Top and bottom panels of the insets provide a cross section and a top view, respectively, for the initial coadsorbed state, transition state, and final state. The reference zero of the energy scale corresponds to the energy of two H atoms in the gas phase at infinite separation from each other and the metal slab. ZPEs are not included. E^* denotes the activation energy barrier for the H_2 recombinative desorption step.

The activation energy barrier required for this step, including the 0.17 eV repulsive interaction between the coadsorbed CO and O, is 0.82 eV (Table 3).

2.2. CO Oxidation by OH: Carboxyl Formation (CO* + OH* → COOH* + *). Direct CO oxidation by OH to produce surface carboxyl species represents a viable alternative to the
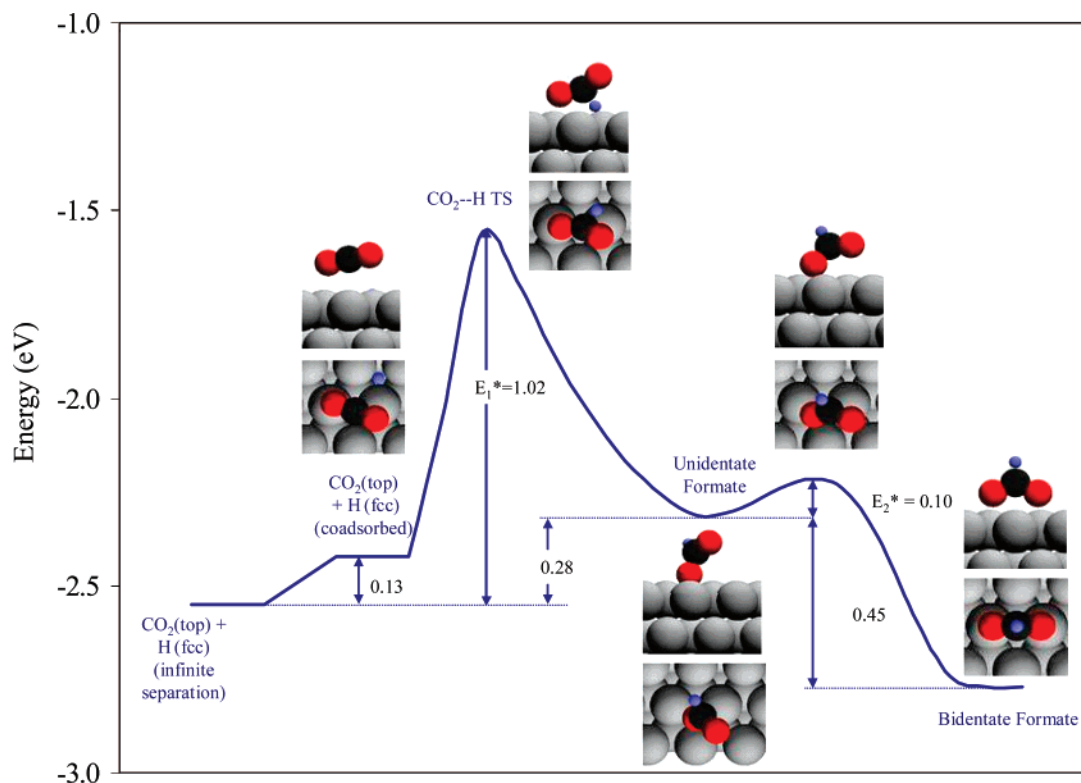
Figure 6. Formate formation. Reaction coordinate for formate formation from CO_2 and adsorbed H. Top and bottom panels of the insets provide a cross section and a top view, respectively, of the initial coadsorbed state, transition state, and final state. The reference zero of the energy scale corresponds to the energy of formate species in the gas phase. ZPEs are not included. Activation energy barriers for unidentate formate formation (E_1^*) and for its transformation to bidentate formate (E_2^*) are shown.

CO + O step. The energetics of COOH formation is shown in Figure 3 (red line). This step is practically thermoneutral, and its overall barrier is smaller than that for CO + O → CO_2. In particular, we find that (i) in the presence of OH, CO prefers to bind at the top site, and (ii) COOH formation is a two-step process in which CO and OH first combine to give the carboxyl species with the O−H bond pointing away from the surface (*cis*-COOH; Figure 1g). Then, *cis*-COOH may undergo a structural transformation to the more stable *trans*-COOH (Figure 1h). The latter step is exothermic by 0.23 eV (Figure 3). *cis*-COOH formation has a barrier of 0.61 eV, whereas *cis*-COOH to *trans*-COOH isomerization is activated by 0.52 eV.

2.3. Carboxyl Dissociation (COOH* + * → CO_2* + H*). The minimum energy path is shown in Figure 4 (blue line). This step is exothermic by 0.39 eV, with a significant activation energy barrier (1.41 eV). At the transition state, the dissociating O−H bond length is 1.33 Å.

2.4. Carboxyl Disproportionation by Hydroxyl (COOH* + OH* → CO_2* + H_2O*). This elementary step is exothermic by 0.40 eV. A remarkable change in the bonding and orientation of COOH and OH species is found upon their coadsorption, leading to their destabilization by 0.39 eV. Importantly, we find that this elementary step is practically spontaneous (with a barrier of only 0.03 eV). Finally, the products of this reaction can be further stabilized by 0.49 eV, accounting for their repulsion energy at the coadsorbed state.

3. H_2 Recombination on Cu(111) (H* + H* → H_2 (g) + 2*). H_2 recombination is endothermic by 0.53 eV. Our calculations show that H_2 does not adsorb molecularly on Cu(111). Figure 5 shows the reaction coordinate for H_2 recombination on Cu(111). Coadsorption of H atoms on two hcp sites (shown

in Figure 5) or two fcc sites is isoenergetic and includes a 0.07 eV repulsion. Including that repulsion yields a barrier of 1.07 eV for H_2 recombination; H_2 dissociation, the reverse reaction, has a barrier of 0.54 eV (Table 3). At the transition state, the H atoms are over bridge sites and the H−H bond length is 1.02 Å (Table 3).

4. Formate Formation on Cu(111). We find that formate can be formed in three different ways: (1) via the direct hydrogenation of CO_2 (CO_2* + H* → HCOO**), (2) through H-transfer from OH to CO_2 (CO_2* + OH* + * → HCOO** + O*), and (3) through H-transfer from H_2O to CO_2 (CO_2* + H_2O* + * → HCOO** + OH*). Although we have studied the energetics of all three steps (Table 3), here we will give a detailed description of only one route, namely the reaction between CO_2 and surface H, which came out to be the most relevant for formate formation.

We find that formate formation from CO_2 and H* is a two-step process. CO_2 and H* first form a unidentate formate that binds to the surface through a single O atom. This step is endothermic by 0.28 eV and has a barrier of 1.02 eV. At the transition state, we find that the C−H bond length is 1.50 Å (Table 3). The conversion of unidentate formate to its bidentate isomer is exothermic by 0.45 eV and is practically spontaneous (with a barrier of 0.10 eV). Table 2 shows that the C−H bond length in the unidentate and bidentate formate is identical. This transformation mainly involves the formation of a second Cu−O bond along with the diffusion of the unidentate formate from the hcp site to a top−top configuration.

Table 3. Thermochemical and Kinetic Parameters for the Elementary Steps Involved in WGSR on Cu(111)[a]

Step No.	Elementary Step	Vibrational modes of Transition State (cm⁻¹)	Bond Lengths in Transition State		Interaction Energy on coadsorption (eV)		Activation Energy (eV)			Frequency Factor at 190°C, A_o s⁻¹
			Bond	Bond Length (Å)	Reactants	Products	E_f	E_r	E_a	
1	CO + * → CO*	--	-	-	-	-	0	0.51 ($\theta \rightarrow 0$)	0.51	
2	H_2+2* → 2H*	1425, 603	H–H	1.02	-	0.07	0.54	1.07	0.50	Collision theory used
3	H_2O+* → H_2O*	--	-	-	-	-	0	0.18	0.18	
4	CO_2+* → CO_2*	--	-	-	-	-	0	0.09	0.09	
5	H_2O*+* → OH*+H*	3689, 1163, 616, 527	O–H	2.23	-	0.36	1.36	1.35	1.15 (0.98)	6.75 x 10¹⁴ (7.34 x 10¹⁵)
6	OH* + * → O* + H*	1409	O–H	1.61	-	0.58	1.76	1.28	1.19	1.54 x 10¹³
7	2 OH* → H_2O* + O*	3786, 1843, 1013, 1139, 725, 505	O–H 2.00 / O–H 1.28	2.00 / 1.28	-0.01	-0.60	0.60	0.00	0.00	2.37 x 10¹⁴
8	CO*+O* → CO_2*+*	2186, 501	C–O	1.93	0.17	-	0.82	1.69	0.79	8.39 x 10¹²
9	CO*+OH* → cis-COOH*+*	3689, 1968, 788, 531	OC–OH	1.81	0.26	-	0.61	0.59	0.55	1.08 x 10¹²
10	cis-COOH* → COOH*	3671, 1709, 978, 886,641	-	-	-	-	0.52	0.75	0.48	9.96 x 10¹²
11	COOH*+* → CO_2*+H*	2046, 1213, 838, 664	O–H	1.33	-	0.03	1.41	1.80	1.18	1.50 x 10¹³
12	COOH* + OH* → CO_2* + H_2O*	3750, 1732, 1609, 1310, 1168, 874, 816, 565	O–H 1.22 / O–H 1.17	1.22 / 1.17	0.39	0.49	0.42	0.82	0.38	5.86 x 10¹⁴
13	CO_2* + H* → HCOO* + *	1996, 1299, 1140, 891,715,538	C–H	1.50	0.13	-	1.02	0.74	0.54	2.23 x 10¹³
14	HCOO* +* → HCOO**	2924, 1640, 1295, 1218, 982, 704	-	-	-	-	0.10	0.55	0.04	8.26 x 10¹²
15	CO_2* + H_2O* + * → HCOO** + OH*	3893, 3778, 2353,1520, 1288, 535	C–H 1.73 / O–H 2.35	1.73 / 2.35	-0.08	0.32	1.69	1.83	1.61	2.83 x 10¹³
16	CO_2*+OH*+* → HCOO**+O*	2551, 1653, 1136, 1235, 915, 641	C–H 1.33 / O–H 1.86	1.33 / 1.86	-0.06	0.67	2.02	1.75	1.71	3.18 x 10¹³

[a] All the parameters listed are calculated using DFT unless otherwise stated. For the transition states, only the vibrational modes above 500 cm⁻¹ are shown; however, all the vibrational modes are considered for calculating frequency factors (A_o). E_f and E_r represent the forward and reverse activation energy, without ZPE corrections, with coadsorbed species at infinite separation from each other. For all the reaction steps, except H_2 dissociation, the frequency factors and the ZPE-corrected values of the activation energies (E_a) for the reaction taken in the exothermic direction are used for defining the microkinetic model. Collision theory is used to calculate the CO, CO_2, and H_2O adsorption rates, as well as the dissociative adsorption of H_2. Shaded entries represent the DFT-determined values that need to be changed to fit the microkinetic model to the experimental data; entries in parentheses indicate the values used in the model.

Discussion

Structure and Energetics of Adsorbed Intermediates. Our DFT calculations show that the binding energy of H on Cu(111) is −2.55 eV, in excellent agreement with the estimate from Redhead analyses of TPD data (−2.45 ± 0.05 eV).[65] Previous DFT studies also give similar BE values: −2.37 eV for $\theta =$ 1/9 ML[66] and −2.39 eV on a relaxed four-layered slab for $\theta =$ 1/4 ML.[67] Our H-site preference for threefold sites compares

well with previous theoretical,[66−69] IRAS,[70] and HREELS[71] studies. We find that O binds to Cu(111) with a BE of −4.41 eV (θ = 1/4 ML). For the same coverage, previous periodic DFT studies reported a BE of −4.29 eV (relaxed slab),[72] −4.56 eV (static slab),[73] and −4.50 eV using LDA pseudopotentials.[74]

(65) Kammler, T.; Küppers, J. *J. Chem. Phys.* **1999**, *111*, 8115.

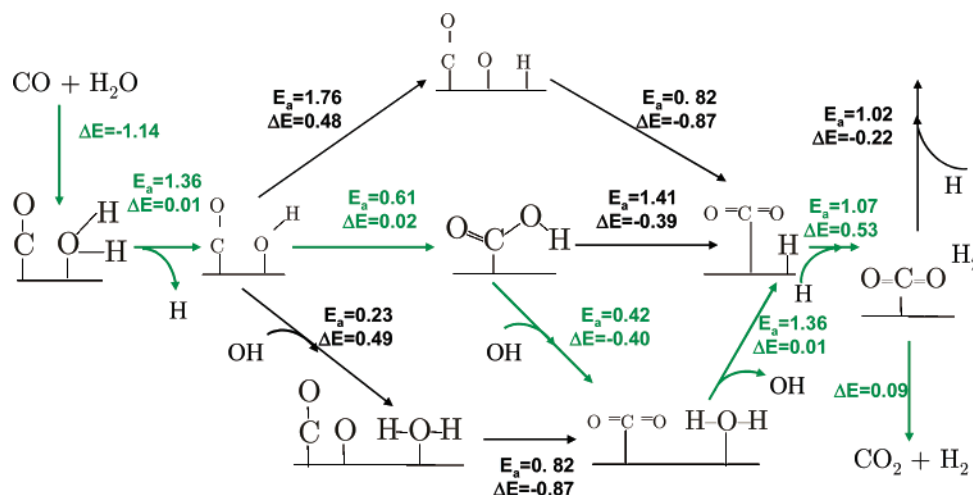(66) Greeley, J.; Mavrikakis, M. *J. Catal.* **2002**, *208*, 291.
(67) Gokhale, A. A.; Huber, G. W.; Dumesic, J. A.; Mavrikakis, M. *J. Phys. Chem. B* **2004**, *108*, 14062.
(68) Gomes, J. R. B.; Gomes, J. A. N. F.; Illas, F. *Surf. Sci.* **1999**, *443*, 165.
(69) Koper, M. T. M.; van Santen, R. A. *J. Electroanal. Chem.* **1999**, *472*, 126.
(70) Lamont, C. L.; Persson, B. N. J.; Williams, G. P. *Chem. Phys. Lett.* **1995**, *243*, 429.

Figure 7. Reaction network for WGSR. A reaction scheme including both the surface redox mechanism and the carboxyl mechanism is outlined. The thermochemistry and the kinetic barriers for all the elementary steps are given in electronvolts. For reactions involving bond making, the activation barriers are reported with respect to the adsorbed reactants at infinite separation from each other. The minimum energy pathway for the WGSR is highlighted with green.

CO binds with a BE of -0.96 eV ($\theta = 1/4$ ML). This BE is significantly higher than that obtained from Redhead analyses of TPD data[75,76] (-0.52 ± 0.05 eV). Additional calculations that we performed for the adsorption of CO on Cu(111) as a function of coverage (θ_{CO}) yields the following correlation: $BE_{CO} = 6.81\theta_{CO}^2 - 3.14\theta_{CO} - 0.53$ (eV). Therefore, for low CO coverages (i.e., $\theta_{CO} \rightarrow 0$), the binding energy of CO is predicted to be ca. -0.51 eV (after ZPE corrections). OH, the other diatomic species studied, binds to the threefold sites with -2.85 eV. This is identical to that determined by previous periodic DFT calculations.[67] Cluster DFT studies[69] also predict a binding energy of -3.01 eV, in reasonable agreement with our results.

Formate (HCOO) has been extensively studied on Cu(111). IRAS, HREELS, STM, and EXAFS studies[39−43] all provide evidence for a bidentate structure, similar to the one we calculated. The BE we calculated for HCOO (-2.77 eV) is in reasonable agreement with that predicted by cluster DFT calculations[68] (-2.99 eV). The existence of unidentate formate has been predicted on Ag surfaces[77] but not on Cu. This may simply reflect the fact that the transformation of unidentate to bidentate formate is almost spontaneous and the latter is significantly more stable than the former on Cu(111). Last, we note that there is no previous proposal or study for carboxyl intermediate on Cu, which we could compare our results against.

Elementary Steps

1. Water Activation on Cu(111).
1.1. H Abstraction from H$_2$O (H$_2$O* + * → H* + OH*). The activation energy barrier for this step is calculated to be 1.36 eV, clearly higher than the barrier to molecular H$_2$O

desorption (0.18 eV). This is in qualitative agreement with prior experimental studies[18,22,27] indicating that it is easier to desorb than to dissociate H$_2$O on Cu(111) and Cu(110) surfaces. DFT studies on cluster models[35] and microkinetic modeling work[16,17] have estimated this barrier to be 1.18 eV. Interestingly, the ZPE-corrected value of our calculated barrier is 1.15 eV (Table 3). We note here that our calculations for this elementary step on a Cu(211) step-edge yield a nearly identical activation energy barrier, suggesting that the specific bond-breaking event may be quasi structure-insensitive. This result is similar to what was found for O$_2$ dissociation on Cu(111) and Cu(211) surfaces.[78]

1.2. OH Dissociation (OH* + * → O* + H*). OH dissociation is endothermic by 0.48 eV and has a significant activation energy barrier of 1.76 eV. These values agree well with results of previous periodic DFT calculations.[79] Earlier microkinetic modeling studies[16] reported a barrier of 1.03 eV for this step. However, the pre-exponential factor used for this step in that model was of O(10^8), whereas our detailed calculations of vibrational frequencies (initial and transition state)[48,49] suggest that this factor is of the O(10^{13}) (Table 3). Therefore, this discrepancy in the barriers might reflect differences in the pre-exponential factors.

1.3. OH Disproportionation (OH* + OH* → H$_2$O* + O*). OH disproportionation (to H$_2$O* and O* at infinite separation from each other) is endothermic by 0.49 eV, very similar to that of OH* + * → O* + H*. However, this step is kinetically favored over the dissociation step, since its activation energy barrier is only 0.23 eV (or 0.6 eV, if H$_2$O* and O* at infinite separation from each other are taken as the final state), versus 1.76 eV for the dissociation step (Figure 2). Earlier experimental studies on Cu(110) and Cu(111) and microkinetic modeling on supported copper catalysts[16,79] have shown that OH disproportionation is preferred to its dissociation.[23,27] We note here that, upon coadsorption, H$_2$O* and O*, the products of OH disproportionation, experience a very strong attractive interaction,

(71) Lee, G.; Plummer, E. W. *Surf. Sci.* **2002**, *498*, 229.
(72) Xu, Y.; Mavrikakis, M. *Surf. Sci.* **2001**, *494*, 131.
(73) Zhang, C. J.; Baxter, R. J.; Hu, P.; Alavi, A.; Lee, M.-H. *J. Chem. Phys.* **2001**, *115*, 5272.
(74) Hammer, B.; Nørskov, J. K. In *Chemisorption and Reactivity on Supported Clusters and Thin Films;* Lambert, R. M., Pacchioni, G., Eds.; Kluwer Academic Publishers: Dordrecht, The Netherlands, 1997; Vol. 331, pp 285−352.
(75) Kirstein, W.; Krüger, B.; Thieme, F. *Surf. Sci.* **1986**, *176*, 505.
(76) Bönicke, I.; Kirstein, W.; Spinzig, S.; Thieme, F. *Surf. Sci.* **1994**, *313*, 231.
(77) Sault, A. G.; Madix, R. J. *J. Phys. Chem.* **1986**, *90*, 4723.

(78) Xu, Y.; Mavrikakis, M. *Surf. Sci.* **2003**, *538*, 219.
(79) Kandoi, S.; Gokhale, A. A.; Grabow, L. C.; Dumesic, J. A.; Mavrikakis, M. *Catal. Lett.* **2004**, *93*, 93.

which tends to stabilize the product state by 0.60 eV, driving the reaction in the forward direction substantially (Table 3 and Figure 2).

2. CO Oxidation on Cu(111).

2.1. CO Oxidation by O ($CO^* + O^* \rightarrow CO_2^* + ^*$). A number of experimental and theoretical investigations of CO oxidation have been performed. Campbell and co-workers estimated a barrier between 0.78 and 0.91 eV on Cu(111) and Cu(110).[18,27] Other experimental studies[80,81] estimated a barrier between 0.78 and 0.86 eV, whereas fitting of experimental data for WGS on Cu-based supported catalysts through microkinetic modeling[1,10,16,17,30,82] leads to a barrier between 0.66 and 0.83 eV for this step. The barrier determined here (0.82 eV) agrees well with these values.

2.2. Carboxyl Formation ($CO^* + OH^* \rightarrow COOH^* + ^*$). Coadsorption of CO and OH on Cu(111) leads to a change in the site preference of CO from the fcc site to the top site. The activation energy barrier to *cis*-carboxyl, with respect to coadsorbed CO^* and OH^*, is only 0.35 eV. This barrier is considerably lower than the corresponding barrier for CO^* oxidation by atomic O^* (0.65 eV), suggesting that, despite being thermodynamically less favorable than CO_2 formation, carboxyl formation is kinetically more accessible.

The atomic-scale details of the reaction coordinate for CO oxidation by either OH or O indicate that it is the oxidizing agent (O or OH) that has to diffuse toward CO for the reaction to happen. This suggests that the OH and O diffusion barriers on Cu(111) may contribute significantly to the activation energy for CO oxidation. In fact, previous periodic DFT studies[67] have estimated those diffusion barriers to be 0.20 and 0.55 eV, respectively, which could account for the difference in the CO oxidation barrier with OH vs O, as reported here.

The isomerization of the *cis*-carboxyl to the more stable *trans*-carboxyl has a barrier of 0.52 eV. During this transformation, the carbonyl O comes closer to the surface, leading to a decrease in the double bond character of the carbonyl C−O bond, as indicated by the increase in the respective C−O bond length (Table 2).

The overall reaction of *trans*-carboxyl formation from CO^* and OH^* is quasi-thermoneutral, whereas both OH dissociation and OH disproportionation steps, which could compete with COOH formation for OH consumption, are endothermic by ca. 0.5 eV. Therefore, COOH formation would be preferable on thermochemical grounds. Furthermore, as pointed out earlier, the effective barrier for OH disproportionation is 0.60 eV, which is comparable to COOH formation barrier. However, since OH disproportionation is second order with respect to OH^*, and as we will discuss subsequently, OH coverage under WGS conditions is very limited, COOH formation wins over OH + OH, as far as OH consumption rate is concerned.

2.3. Carboxyl Decomposition. Carboxyl dissociation ($COOH^* + ^* \rightarrow CO_2^* + H^*$) is exothermic by 0.39 eV with an activation energy barrier of 1.41 eV. Clearly, Figure 4 shows that carboxyl disproportionation with OH^* ($COOH^* + OH^* \rightarrow CO_2^* + H_2O^*$) offers a much more viable alternative route to $COOH^*$ decomposition. The disproportionation step is exothermic by

0.40 eV, but has a much lower activation energy barrier (0.42 eV) than the $COOH^* + ^* \rightarrow CO_2^* + H^*$ step. When coadsorbed with OH, we find that carboxyl and OH show a change in the orientation (Figure 4). This results in destabilizing the adsorbed intermediates by 0.39 eV. At the same time, hydrogen bonding is developed between $COOH^*$ and OH^*, which tends to facilitate the transfer of H from COOH to OH toward water formation. The reaction between coadsorbed carboxyl and OH is practically spontaneous. We note in passing that we have also investigated $COOH^* + O^* \rightarrow CO_2^* + OH^*$, but because of the unfavorable energetics compared to that of $COOH^* + OH^* \rightarrow CO_2^* + H_2O^*$ and the lack of atomic O^* under realistic WGS conditions (see discussion in the Microkinetic Model section), we do not expand on the details of that elementary step here.

3. H_2 Recombination ($H^* + H^* \rightarrow H_2$ (g) + 2*). This is an endothermic step ($\Delta E = 0.53$ eV) with an activation energy barrier of 1.07 eV. The relatively high barrier suggests that under typical low-temperature WGS conditions considerable H coverage may be expected. H_2 dissociation on Cu(111) has been studied extensively by Hammer et al.[83] They determined an activation energy barrier of 0.55 eV, which agrees very well with our findings (0.54 eV; Table 3).

4. Formate Formation. We have investigated three different elementary steps for formate formation. Of these steps, the reaction between CO_2 and surface OH ($CO_2^* + OH^* + ^* \rightarrow HCOO^{**} + O^*$) and the reaction between CO_2 and H_2O ($CO_2^* + H_2O^* + ^* \rightarrow HCOO^{**} + OH^*$) present a substantially higher barrier than the direct hydrogenation of CO_2 ($CO_2^* + H^* \rightarrow HCOO^{**}$) (Table 3). Therefore, here we discuss only the latter mechanism. We find that formate formation from CO_2 and surface H is a two-step process: (1) a unidentate formate is formed, and (2) unidentate formate transforms to its more stable bidentate isomer. Although unidentate formate has not been detected on Cu(111) surface, its presence has been shown on Ag(110).[77] Our calculations show that the barrier to unidentate formate formation is 1.02 eV (Figure 6). The bidentate formate is more stable than its unidentate isomer by ca. 0.45 eV (Table 2). The transformation of unidentate to bidentate formate is activated by only ca. 0.1 eV, a nearly spontaneous process under typical reaction conditions. Thus, unidentate formate is likely to be an extremely short-lived species on Cu(111).

TPR studies[28,29,34,84,85] on single crystal Cu and Cu/SiO₂ catalysts have suggested the barrier for dissociation of formate to be between 1.03 and 1.22 eV. The overall activation energy for formate dissociation calculated here (1.18 eV) is in good agreement with these estimates.

The barrier for formate formation is significantly lower than the barrier for H_2O dissociation, suggesting that formate formation should proceed under typical low-temperature WGSR conditions. In a subsequent section, we will validate this tentative suggestion through a detailed microkinetic modeling analysis of experimental WGSR data. In particular, we find that formate covers a significant fraction of Cu(111) under typical WGSR conditions and that this coverage increases with the partial pressure of CO_2 and H_2, implying that formate coverage

(80) Habraken, F. H. P. M.; Mesters, C. M. A. M.; Bootsma, G. A. *Surf. Sci.* **1980**, *97*, 264.
(81) Habraken, F. H. P. M.; Kieffer, E. P.; Bootsma, G. A. *Surf. Sci.* **1979**, *83*, 45.
(82) Waugh, K. C. *Catal. Today* **1999**, *53*, 161.

(83) Stromquist, J.; Bengtsson, L.; Persson, M.; Hammer, B. *Surf. Sci.* **1998**, *397*, 382.
(84) Nerlov, J.; Chorkendorff, I. *J. Catal.* **1999**, *181*, 271.
(85) Yatsu, T.; Nishimura, H.; Fujitani, T.; Nakamura, J. *J. Catal.* **2000**, *191*, 423.

is governed almost entirely by the equilibrium of the reaction between CO_2 and surface H.

## Potential Energy Surface for WGSR on Cu(111)

The thermochemistry and activation energy barriers of various elementary steps discussed in the previous sections can be summarized in the reaction network shown in Figure 7. On the basis of the DFT-derived energetics alone, one can suggest that the minimum energy path for WGSR on Cu(111) goes through the formation of carboxyl intermediate, followed by its disproportionation with a surface OH. The energetics of the conventionally accepted redox mechanism is clearly worse than that of the COOH-mediated mechanism.

Microkinetic Model

All 16 elementary steps shown in Table 3 are included in a microkinetic model. A total of 52 parameters, including binding energies and entropies of surface intermediates, activation energy barriers, and frequency factors, are required by the model. The initial estimates for the ZPE-corrected binding energies and activation energies are obtained from the DFT calculations described above. Entropies of adsorbed intermediates and frequency factors are determined from the DFT-calculated vibrational frequencies following a procedure described elsewhere.[48,49] Entropies and heats of formation of gas-phase species are obtained from standard references.[86]

A summary of the various parameters used in the microkinetic model is contained in Tables 2 and 3. To account for the coverage dependence of the heat of adsorption for CO, we fitted a polynomial to the DFT-derived binding energy of CO (BE_{CO}) at various coverages (θ_{CO}), ($BE_{CO} = 6.81\theta_{CO}^2 - 3.14\theta_{CO} - 0.53$ eV) and ZPE-corrected this BE_{CO}; as a result, the BE_{CO} at the zero-coverage limit is -0.51 eV. We note here that elementary steps involving formate, such as $CO_2* + OH* + * \rightarrow HCOO** + O*$ and $CO_2* + H_2O* + * \rightarrow HCOO** + OH*$, are also incorporated into the microkinetic model, despite the fact that they were not discussed in detail above. Nevertheless, activation energies and frequency factors for these steps were determined rigorously within the framework of our DFT studies (Table 3). Interestingly, very recent work has shown that attractive H_2O/OH hydrogen-bonding interactions can play a considerable role in H_2O adsorption/desorption and dissociation kinetics at near-ambient conditions.[87,88] Such effects have not been included in this work.

Using the DFT-derived parameters as initial estimates for the model parameters, we fitted the 16-step model described above to the experimental WGSR rate data published by Koryabkina et al.[10] This data has been collected in a CSTR reactor at 463 K, 1 bar, and with the feed containing varying proportions of CO, CO_2, H_2O, and H_2. We find that the values for the activation energies, binding energies, frequency factors, and entropies determined using our DFT studies do an excellent job of describing the experimental data. Only a few parameters (BE_H, BE_{HCOO}, and E^* for H abstraction from H_2O; see shaded entries in Tables 2 and 3) needed to be slightly changed from their
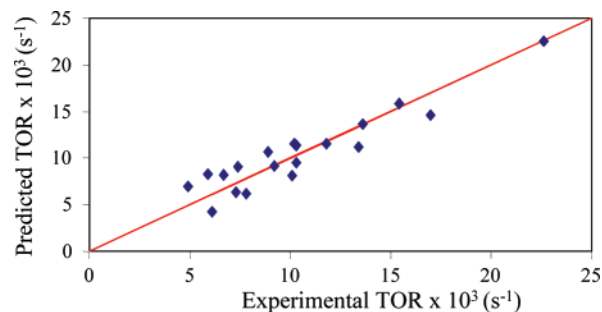
Figure 8. Experimental WGSR rates versus rates predicted by the microkinetic model experimental data were taken from Koryabkina et al.[10]

DFT-determined values to fit the kinetic data, and these changes are all within the error bars of DFT calculations (ca. ± 0.1 eV). Figure 8 provides a parity plot between the experimental turnover rates (TORs) and those predicted by our DFT-based microkinetic models. Deviations from the parity line represent the error involved in predicting the experimental rates by using our model. Therefore, we conclude that the DFT-derived parameters for all the elementary steps for WGSR on Cu(111) appear to describe the reaction mechanism very well.

Furthermore, we test our model against the kinetic data collected by Herwijnen and Jong on a $Cu/ZnO/Al_2O_3$ catalyst.[38] Their experiments probed the effect of temperature and CO and H_2O concentrations on reaction rates by varying the concentrations of the reactants at five different temperatures in a plug flow reactor. We find that our DFT-based microkinetic model predicts experimental reaction rates under these very diverse reaction conditions exceptionally well.

The very good agreement between the microkinetic modeling rates and the experimentally reported rates, as shown in Figure 8, suggests that Cu(111) may be a dominant active site for WGS on realistic industrial catalysts based on $Cu/ZnO/Al_2O_3$. An alternative explanation may be that the WGS reaction on the specific catalysts is not very structure sensitive, and therefore the reaction rate is comparable on different Cu facets. On the basis of our results, we may also suggest that ZnO/Al_2O_3 does not play a major role in determining reaction rates on these catalysts.

Dominant Reaction Mechanism. Having established that our microkinetic model predicts experimental WGS reaction rates well, we then turn our attention into exploring information provided by the model itself. A comparison of the relative rates of the various elementary steps included in the model reveals (i) the rates of carboxyl formation steps (steps 9 and 10 in Table 3) and carboxyl reaction with OH (step 12 in Table 3) are almost the same as the net rate for the overall WGSR, and (ii) the rates of OH dissociation, OH disproportionation, and CO oxidation by O (steps 6−8 in Table 3) are all negligible compared to the overall WGSR rate. These results clearly suggest that the dominant reaction mechanism involves CO oxidation by OH to form carboxyl, followed by the decomposition of COOH through a disproportionation reaction with OH. The surface redox mechanism does not play a significant role in the WGSR mechanism. The new COOH-mediated WGSR mechanism provides a mechanistic bridge for this reaction between homogeneous[44−46] and heterogeneous catalysis.

Rate-Limiting Step and the Role of Formate. Within the framework of the DFT-parametrized microkinetic model, we

(86) Lindstrom, B.; Pettersson, L. *J. Int. J. Hydrogen Energy* **2001**, *26*, 923.
(87) Yamamoto, S.; Andersson, K.; Bluhm, H.; Ketteler, G.; Starr, D. E.; Schiros, T.; Ogasawara, H.; Pettersson, L. G. M.; Salmeron, M.; Nilsson, A. *J. Phys. Chem. C* **2007**, *111*, 7848.
(88) Andersson, K.; Ketteler, G.; Bluhm, H.; Yamamoto, S.; Ogasawara, H.; Pettersson, L. G. M.; Salmeron, M.; Nilsson, A. *J. Phys. Chem. C* **2007**, *111*, 14493.

solve the steady-state rate equations for surface coverages of all reactive intermediates. In a subsequent step, using these coverages and the energetics of the elementary steps, we calculate forward and reverse reaction rates and from those the net reaction rate for each of the elementary steps included in the model. Inspection of the net reaction rates allows for the identification of rate-limiting steps.[47,48] Importantly, the rate-limiting step in a reaction network can be determined rigorously using Campbell's degree of rate control.[89] In that formalism, the rate control ($X_{RC,i}$) of each step i is evaluated by:

$$X_{RC,i} = \frac{k_i}{r_{net}} \left(\frac{\delta r_{net}}{\delta k_i} \right)_{K_i, k_{j,j \neq i}}$$

where K_i and k_i denote the equilibrium constant and rate constant for step i, and r_{net} stands for the net reaction rate.

We simulated two different sets of conditions: (a) $P = 1$ bar, $T = 463$ K, and feed composition = 30% CO, 30% H_2O (balance inert), and (b) $P = 1$ bar, $T = 463$ K, and feed composition = 7% CO, 21% H_2O, 8.5% CO_2, and 38% H_2 (balance inert). Our model predicts that under both conditions step 5 ($H_2O^* + * \rightleftharpoons H^* + OH^*$) and step 9 ($CO^* + OH^* \rightleftharpoons cis - COOH^* + *$) are rate controlling. In the absence of CO_2 and H_2 co-feed, step 5 has a considerably stronger influence on the overall reaction rate.

The model shows that only steps 1−5, 9, 10, and 12 (Table 3) contribute to the net reaction rate. Further analysis targeting the forward and reverse rates for the various elementary steps at 463 K and 1 bar pressure, for a feed composition of 7% CO, 21% H_2O, 8.5% CO_2, and 38% H_2 (balance inert), shows that steps 1−4 and 10 are equilibrated, steps 5 and 12 are reversible, and step 9 is irreversible. We also find that steps leading to bidentate formate formation from CO_2 and H (steps 13 and 14 in Table 3) are both equilibrated. This suggests that formate formation is primarily dictated by the thermodynamics of the process, and therefore increasing the partial pressure of CO_2 and H_2 will lead to increased formate coverage. Furthermore, as pointed out earlier and on the basis of the DFT results alone, whereby the activation energies for steps 15 and 16 are significantly higher than those for steps 13 and 14 (Table 3), we suggested that the most likely route for formate formation involves the reaction between CO_2 and H. This estimate appears to be validated completely by the results of our detailed microkinetic model. In particular, we find that, although steps 15 and 16 are almost equilibrated, their forward and the reverse reaction rates are more than 4 orders of magnitude lower than the corresponding rates for steps 13 and 14. Thus, under reaction conditions, formate participates in steps 13 and 14 but no other surface reactions, suggesting that formate plays the role of a spectator species for WGSR on Cu surfaces.

Surface Coverages. Figure 9 shows surface coverages of the most abundant surface intermediates as a function of pressure, at $T = 463$ K and for a feed composition of 7% CO, 21% H_2O, 8.5% CO_2, and 38% H_2 (balance inert). We find that, in the pressure range of 1−20 bar, bidentate formate and atomic H are the most abundant surface intermediates, whereas CO coverages are relatively low (ca. 1%). The coverage of all other species is less than 10^{-4}. As pressure increases, formate coverage increases dramatically, whereas coverages of H and

(89) Campbell, C. T. *J. Catal.* **2001**, *204*, 520.
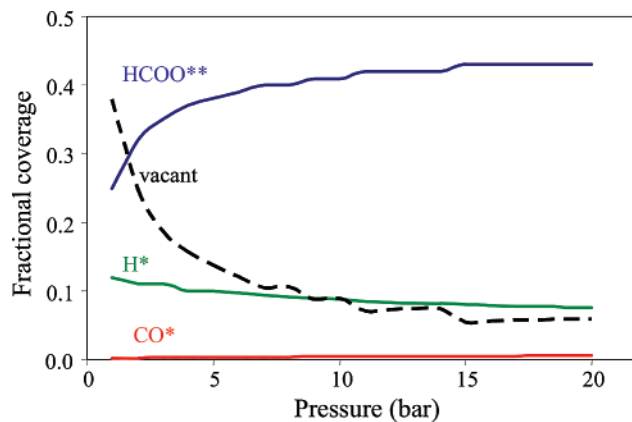
Figure 9. Effect of pressure on the surface coverage of key WGSR intermediates on Cu(111). Microkinetic model predictions for surface coverage of formate (HCOO), hydrogen (H), carbon monoxide (CO), and vacant sites as a function of total pressure for a Cu catalyst operating at 463 K and 118 mL/cc flow of 7% CO, 21% H_2O, 8.5% CO_2, and 38% H_2 with balance inerts. Coverage of other species is $< 10^{-4}$.
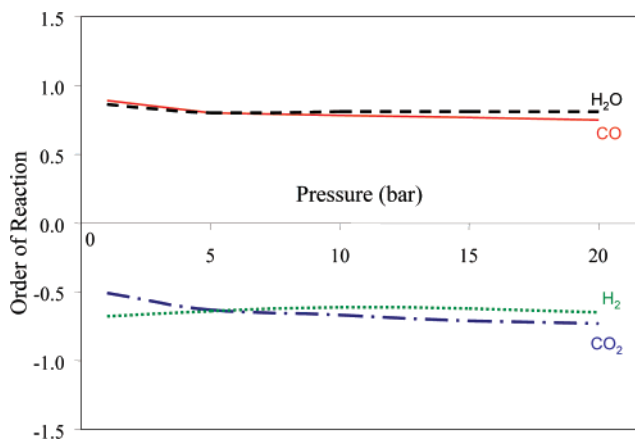
Figure 10. Reaction orders as a function of pressure for WGSR on Cu with respect to CO, H_2O, CO_2, and H_2 for a catalyst operating at 463 K and 118 mL/cc flow of 7% CO, 21% H_2O, 8.5% CO_2, and 38% H_2 (balance inert).

CO remain mostly invariant. Taking into account the coexistence of CO, CO_2, and H_2 over Cu/ZnO catalysts in methanol synthesis, occurring at much higher pressures, our model points to the importance of formate intermediate for that reaction, too.[1,10,17] Interestingly, we find that the carboxyl intermediate, through which WGSR is happening, has extremely low coverage at all pressures, implying that COOH is a very reactive intermediate which might prove difficult to identify spectroscopically.

Reaction Orders. The order α of a reaction with respect to species i is evaluated as follows: $\alpha_i = [\partial(\ln r_{net})]/[\partial \ln(p_i/p_o)]$, where r_{net} is the net reaction rate, and p_i and p_o denote the partial pressure of species i and the total pressure, respectively.

Figure 10 shows the microkinetic-model-predicted order of WGSR on Cu/ZnO/Al_2O_3 with respect to CO, H_2O, CO_2, and H_2 over a range of pressures at 463 K with a feed composition of 7% CO, 21% H_2O, 8.5% CO_2, and 38% H_2 (balance inert). The negative CO_2 and H_2 reaction orders suggest that WGSR is inhibited by its products. Our model predicts that the reaction order with respect to H_2 at 1 bar is ca. −0.7, which agrees reasonably well with the experimentally determined order of about −0.9.[10] One of the problems that previous microkinetic modeling studies had was their inability to capture the negative

reaction order with respect to CO_2, especially at atmospheric pressure.[10,17] These models predicted the CO_2 reaction order to be zero at 1 bar, although experiments consistently pointed to a negative order (ca. -0.9).[10] Our model, including the COOH-mediated WGSR mechanism, improves on that point and predicts a negative CO_2 reaction order (ca. -0.55). Furthermore, as shown in Figure 10, WGSR is inhibited increasingly by CO_2 with increasing pressure. This is because progressively more formate is formed on the surface, blocking more active sites. In contrast, we have shown that H coverage does not change much with pressure (Figure 9), which is in accord with our prediction that the reaction order with respect to H_2 is not a strong function of pressure (Figure 10). Similarly, increasing pressure has practically no effect on CO and H_2O reaction orders (Figure 10). At 1 bar, our model predicts the CO order to be ca. 0.90, when experimental studies suggest a ca. 0.8 order.[10] The same experiments suggest a H_2O order of 0.8, when our model predicts ca. 0.85 (at 1 bar).

Apparent Activation Energy. In general, the apparent activation energy is a function of temperature, pressure, and feed composition. Using our microkinetic model, we can determine the apparent activation energy as $H^* = k_BT^2[\partial \ln(r_{net})/\partial T]_P$, where r_{net} represents the net reaction rate, T the reaction temperature, P the pressure, and k_B the Boltzmann constant.

Experimental studies by Herwijnen and Jong[38] at 1 bar have estimated a WGSR apparent activation energy of 69 kJ/mol for a feed of 21% CO and 54% H_2O (balance inert). For these conditions, our model predicts the apparent activation energy of 67 kJ/mol. Similarly, our model predicts an apparent activation energy of 78 kJ/mol at 1 bar and 463 K for a feed of 7% CO, 21% H_2O, 8.5% CO_2, and 38% H_2 (balance inert), which is reasonably close to the experimentally reported value of 70 kJ/mol for these conditions.[10]

Conclusions

We have presented a detailed DFT analysis of all the elementary steps implicated in the redox and a new carboxyl-mediated mechanism for the low-temperature WGS reaction on Cu(111). Thermochemical parameters, entropies, frequency factors, and activation energy barriers of all elementary steps were calculated from first principles. The energetics of compet-

ing reaction paths point to the predominance of the COOH-mediated WGS path, whereby CO is directly oxidized by surface OH, rather than atomic O. A detailed microkinetic model accounting for all these elementary steps was constructed and used to calculate reaction rates under realistic WGS reaction conditions. Two sets of experimental data, covering a wide range of temperature, pressure, and feed compositions, were successfully reproduced by the microkinetic model, when the DFT-derived parameters were utilized. The model confirmed that the dominant WGS reaction path goes through the formation of the carboxyl intermediate, followed by its decomposition via disproportionation with surface OH. According to our results, the commonly accepted redox mechanism, also included in our model and occurring via the CO + O oxidation step, plays no significant role in WGS on Cu catalysts.

Importantly, we found that, on Cu(111): (1) H abstraction from H_2O appears to be the rate-controlling step for the entire WGS reaction network, (2) carboxyl (COOH) is a very reactive intermediate, short-lived, and likely difficult to be identified spectroscopically, and (3) formate (HCOO), formed from CO_2 + H, is a spectator species which tends to block active sites, and can reach substantial surface coverages, particularly at higher pressures. This site blocking by formate can explain the observed negative WGS reaction order with respect to CO_2.